

Mutual information for fermionic systems

Luca Lepori,^{1,2} Simone Paganelli,³ Fabio Franchini,⁴ and Andrea Trombettoni^{5,6,7}

¹*Dipartimento di Fisica, Università della Calabria, Arcavacata di Rende I-87036, Cosenza, Italy*

²*I.N.F.N., Gruppo collegato di Cosenza, Arcavacata di Rende I-87036, Cosenza, Italy*

³*Dipartimento di Scienze Fisiche e Chimiche, Università dell'Aquila, via Vetoio, I-67010 Coppito-L'Aquila, Italy*

⁴*Ruder Bošković Institute Bijenčka cesta 54, 10000 Zagreb, Croatia*

⁵*Department of Physics, University of Trieste, Strada Costiera 11, I-34151 Trieste, Italy*

⁶*SISSA and I.N.F.N., via Bonomea 265, I-34136 Trieste, Italy*

⁷*CNR-IOM DEMOCRITOS Simulation Center, Via Bonomea 265, I-34136 Trieste, Italy*

We study the behavior of the mutual information (MI) in various quadratic fermionic chains, with and without pairing terms and both with short- and long-range hoppings. The models considered include the short-range Kitaev model and also cases in which the area law for the entanglement entropy is – logarithmically or non-logarithmically – violated. When the area law is violated at most logarithmically, the MI is a monotonically increasing function of the conformal four-point ratio x , also for the Kitaev model. Where non-logarithmic violations of the area law are present, then non-monotonic features of MI can be observed, with a structure of peaks related to the spatial configuration of Bell pairs, and the four-point ratio x is found to be not sufficient to capture the whole structure of the MI. For the model exhibiting perfect volume law, the MI vanishes identically. For the Kitaev model, when it is gapped or the range of the pairing is large enough, then the results have vanishing MI for small x . A discussion of the comparison with the results obtained by the AdS/CFT correspondence in the strong coupling limit is presented.

1. INTRODUCTION

Over the years, information theory has provided valuable tools to analyze and interpret many-body quantum systems. The entanglement entropy (EE), as measured by the von Neumann and Renyi entropies, has quickly established itself as a standard benchmark that allows to discriminate different phases of matter and properties escaping traditional paradigms. EE provides relevant knowledge such as how much classical information is necessary for a faithful representation of a quantum system or as an efficient witness of critical behavior [1, 2].

The EEs are bipartite measures, since they assess how much information is shared between two complementary subsystems of a system in a pure state (that is, with no intrinsic entropy as a whole). This information cannot be accessed by measurements on one part alone, as it reflects correlations between the two subsystems. Since correlations lie mostly on the boundaries between the subsystems, the area law, at most with logarithmic corrections, is typically obeyed [3].

To access additional information on the structure of multipartite entanglement and quantum correlations, multipartite measures have also been introduced. One such measure, although not an entanglement estimator, is the so-called *mutual information* (MI). The MI is typically tripartite. Starting with a system in a pure state, one indeed divides the system into two (non-overlapping) subsystems A and B and their complement $C \equiv A \cup B$. The MI measures how much information on A we can obtain by measuring B (or vice-versa). Thus, the MI can be considered as a kind of 2-point function, while, from this point of view, the EEs are essentially 1-point functions. Note, however, that an alternative point of view is to start with a system made only of A and B in a mixed

state obtained by tracing out C and then to calculate the MI between A and its complement $B = \bar{A}$. Comparing the two points of view, the latter can be considered as the result of removing C and let A and B be "immersed" in the bath constituted by C .

Keeping this into account, in this work we will take the former approach and only consider pure tripartite systems, initializing the system under consideration in its (pure) ground state

$$\rho = |\psi_0\rangle \langle \psi_0|. \quad (1)$$

We then divide the lattice in the three disjoint parts A , B and their complement $C = \bar{A} \cup \bar{B}$. The reduced density matrix of each subsystem is given by $\rho_A = \text{tr}_{B \cup C} \{\rho\}$, $\rho_B = \text{tr}_{A \cup C} \{\rho\}$, $\rho_{AB} = \text{tr}_C \{\rho\}$, and $\rho_C = \text{tr}_{A \cup B} \{\rho\}$, respectively. Starting from the von Neumann entropy of the subsystem j , defined as

$$S_j = -\text{tr} \{\rho_j \ln \rho_j\}, \quad (2)$$

(where ρ_j is the reduced density matrix of the subsystem j), the MI between A and B , denoted by $I_{(A,B)}$, is given by

$$I_{(A,B)} = S_A + S_B - S_{AB}. \quad (3)$$

The MI is positive and symmetric in A and B . If A and B are complementary (that is $A \cup B$ equals the entire system) and the whole system is prepared into a pure state, then $S_{AB} \equiv S_{A \cup B} = 0$ and $I_{(A,B)} = 2S_A = 2S_B$, thus the MI reduces to the von Neumann entropy. The MI satisfies an area law [4] and provides an upper bound to any 2-points correlation function computed between A and B :

$$I_{(A,B)} \geq \frac{\left(\langle \mathcal{O}_A \otimes \mathcal{O}_B \rangle - \langle \mathcal{O}_A \rangle \langle \mathcal{O}_B \rangle \right)^2}{2 |\mathcal{O}_A|^2 |\mathcal{O}_B|^2}. \quad (4)$$

Thus, the MI vanishes when no correlation exists between A and B .

In the general case, $I_{(A,B)}$ is independent from UV cut-off parameters (since the divergences of the individual regions cancel over those of their union) and this is one of the properties that renders it more flexible over the entanglement entropy, for which it is sometime complicated to disentangle the physical from the cut-off contributions. Another limitation of the EE is that it makes sense as a measure only if the system is prepared in a pure state, while, as we remarked, the MI applies also to mixed state systems.

The MI can be considered as a kind of 2-point function, since it depends on the relative position of regions A and B . The MI is not a proper entanglement measure. However it is a measure of correlation between subsystems of quantum system, and it quantifies the amount of information shared between the two regions, providing a quantum counterpart of the Shannon MI, which in general quantifies in suitable units the amount of information obtained about a random variable via the measurement of another random variable [5].

The MI has been studied in several prototypical settings, starting from the Ising model [6, 7] and critical chains [8–10], in systems at finite temperature [11–15] and out of equilibrium [16–21]. Moreover, it has been used as a test for several phenomena, for instance in disordered systems [22–24] and in the presence of spontaneous symmetry breaking [25], and as well in the holographic settings [26–29]. In 1D systems described by a CFT, several results have been obtained for the MI calculated with respect to the Shannon entropies (that is, basis dependent entropies) [8–10], while exact results in lattice systems have been obtained only in special cases [30]. We refer to [31] for a review on the EE in free quantum field theory with disjoint intervals.

A general prediction for the behavior of the MI comes from the AdS/CFT correspondence, in the strong coupling (large conformal charge c) limit, where the MI has been found to behave as [26, 27]

$$I_{(A,B)}(x) = \begin{cases} 0, & x < 1/2 \\ \frac{c}{3} \log \frac{x}{1-x}, & x \geq 1/2 \end{cases}, \quad (5)$$

as a function of the conformal four-point ratio x , defined as

$$x = \frac{l^2}{(l+d)^2}, \quad (6)$$

where l is the length (i.e., the number of sites) of the two subsystems A and B (taken of the same size) and, assuming A and B both simply connected. In (5) d is a distance between the two subsystems, being the minimum number of sites between two points belonging to A and B . The four-point ratio is the traditional quantity used in CFT analysis [32] used to encode the position of the four edges of the two subsystems.

Most of the studies of MI have focused so far mostly on systems with short-range couplings/interactions. In this respect it would be interesting to compare results for long-range systems with the corresponding short-range findings, as motivated by recent results for quantum systems with long-range couplings where the effects of long-rangedness on critical properties, quantum dynamics and quantum entanglement properties have been studied [33–42]. One of the models in which the features induced by long-range terms have compared with their short-range counterparts have been subject of considerable effect is the long-range Kitaev model [43–53], where the pairing term present in the short-range chain $\sim \Delta c_i^\dagger c_{i+1}^\dagger$ [54] has the form $\sim \Delta_{ij} c_i^\dagger c_j^\dagger$.

Our goal in the present paper is four-fold: *i*) to compare the short-range Kitaev model with the tight-binding chain to highlight the effect of the pairing term on the MI; *ii*) to study how short-range results for the MI get modified in presence of long-range terms, analyzing the MI in several prototypical 1D chains with long-range hoppings and pairings; *iii*) to discuss the dependence of the MI on the conformal four-point ratio x in the various models, including the Kitaev model; *iv*) to probe the, possibly different, behavior of the MI for systems displaying area law or its (non-logarithmic) violation for the EE. We will consider quadratic and translational invariant fermionic chains, allowing for the study of the MI for large system size [55]. Regarding points *i*) and *iii*), we observe that although the considered models are not in the strong coupling regime of validity of the AdS/CFT result (5), we aim at testing at least a qualitative agreement with it. We will show that, when the area law is violated more than logarithmically, the MI develops non-monotonic features, with peaks for small x , in contrast with (5). We will also argue that the four-point ratio is not sufficient to capture the structure of MI for systems with volume law of EE, indicating an incompatibility of these cases with the assumption of conformal invariance and thus, the failure of both the CFT and holographic predictions.

The plan of the paper is the following. In Sec. 2 we introduce the models we are going to consider. Sec. 3 is devoted to the short-range models, with the tight-binding model considered in Sec. 3.1 and the Kitaev chain in 3.2. Long-range models are considered in Sections 4 and 5: in the former the long-range terms are the hopping ones, while in the latter we study the effect of long-range pairing terms. In Sec. 4 we consider different forms of hoppings characterized by different forms of the EE scaling. Hoppings decaying as a power-law exhibit area law for the EE are considered in Sec. 4, while the MI for model with fractal Fermi surface having a scaling of EE intermediate between area and volume laws is discussed in Sec. 4.1. Models featuring EE law volume are studied in Sec. 4.2, where we consider a long-range power-law model with a space-dependent phase in the hopping [Sec. 4.2.1] and models with selective hoppings where the hopping is chosen in a way to reproduce a state with the maximum number of Bell pairs, therefore giving EE vol-

ume law [Sec. 4.2.2]. We focus in particular on the model in which each site is coupled by an hopping term to the most distant site, a model introduced in [56] and to which we refer as the "antipodal" model. Deviations from the antipodal model are as well investigated. Sec. 5 considers the case of long-range pairings, both with short-range hoppings [Sec. 5.1] and long-range hoppings [Sec. 5.2]. The use of MI to detect quantum phase transitions in such models is studied. Final comments and conclusions drawn from our results are in Sec. 6.

2. THE MODELS

In this paper, we consider 1D fermionic models of the form

$$H = H_H + H_P, \quad (7)$$

where H_H is the hopping part and H_P the pairing part of the Hamiltonian. Sites are labeled by indices $i, j = 1, \dots, N_S$ and N_S is the number of sites. The fermionic operators creating and destroying a fermion in the site i are denoted by c_i and c_i^\dagger , respectively. The filling f is defined as $f = N_T/N_S$ and it is the number of particles per site. As usual, the filling can be fixed directly or via the introduction of a chemical potential μ , amounting to fixing the number of fermions from the Hamiltonian $H - \mu N_T$, where the total number operator is $N_T = \sum_{i=1}^{N_S} c_i^\dagger c_i$. We will consider as well translational invariant models, where, unless explicitly stated, periodic boundary conditions (PBC) are imposed:

$$c_{i+N_S} \equiv c_i. \quad (8)$$

The hopping part H_H of the Hamiltonian (7) reads in general

$$H_H = - \sum_{i,j=1}^{N_S} t_{i,j} c_i^\dagger c_j + \text{h.c.}, \quad (9)$$

where $t_{i,j}$ is the hopping amplitude among sites i and j . Several form of $t_{i,j}$ will be considered:

- a) nearest-neighbor, with $t_{i,j} \neq 0$ for $j = i \pm 1$ and vanishing otherwise;
- b) selective hopping, with $t_{i,j}$ constant and non-vanishing if the distance between i and j is in an assigned interval of values. For instance, the antipodal model has $t_{i,j} \neq 0$ only if $|i - j| = N_S/2$ (with N_S even).
- c) long-range with

$$t_{i,j} \propto \frac{1}{|i - j|_p^\alpha}, \quad (10)$$

where the distance $|\cdot|_p$, due to PBC conditions, is defined as

$$|i - j|_p = \min(|i - j|, N_S - |i - j|). \quad (11)$$

Notice that while in Sections 3.1 and 4 the prefactor not written in (10) is considered real, in the model discussed in Section 4.2.1 is complex.

The power-law exponent α in (10) is such that for $\alpha \rightarrow \infty$ the short-range limit is retrieved. Moreover, if $\alpha > d = 1$ (more in general α larger than the dimension d of the lattice) then the energy is extensive [57]. When $\alpha > 1$, in statistical mechanics models one can find a value of α , often denoted by α^* , such that for $\alpha > \alpha^*$ the critical behavior is the one of the short-range model [58], although of course non-universal quantities may depend on α (see a review in [59]). One refers often to the range $\alpha \leq 1$ as the "strong" long-range" region and to $1 < \alpha < \alpha^*$ as the "weak" long-range region, but in this paper, not being crucially focused on critical properties, we will not make such distinction, making generically reference to the law (10) as a long-range, power-law decay. An important point emerging in the study of lattice models with long-range interactions is that critical properties change with the exponent α at a fixed dimension of the lattice in which interactions are long-range [59]. So, from this point of view, changing the dimension of the lattice (e.g., considering 2D lattices), although interesting, is expected not to qualitatively change the properties we are going to discuss.

Since we are adopting PBC, the eigenfunctions of the matrix $-t_{i,j}$ are plane waves $\psi_k(j) \propto e^{ikj}$, with $k = \frac{2\pi}{N_S} n_k$ and $n_k = -N_S/2, \dots, N_S/2 - 1$, again assuming N_S even (the lattice spacing is set for simplicity $\equiv 1$). Therefore the hopping Hamiltonian (9) can be readily diagonalized as $H_H = \sum_k \epsilon_k c_k^\dagger c_k$, with c_k Fourier transform of c_i and ϵ_k depending of course on the specific form of the $t_{i,j}$. In Sec. 4.1 a model with fractal Fermi surface is studied, and there the form of ϵ_k will be directly given without explicitly assigning the hoppings $t_{i,j}$.

For the hopping Hamiltonian (9) the EE of the subsystem A having l sites is given by [55]

$$S_A = - \sum_{\gamma=1}^l [(1 - C_\gamma) \ln(1 - C_\gamma) + C_\gamma \ln C_\gamma]. \quad (12)$$

In (12) the C_γ are the l eigenvalues of the correlation matrix

$$C_{ij} = \langle \Psi | c_i^\dagger c_j | \Psi \rangle, \quad (13)$$

with $i, j = 1, \dots, l$ being the sites belonging to A and Ψ the ground-state of the fermionic system.

To calculate the MI, we calculate the EE of two systems A and B having each l sites, then the EE of $A \cup B$, and finally the MI using (5). In this way we can readily calculate and analyze the MI, and express it in term of the four-point ratio where d is the (minimal) distance between A and B . The results we are going to present in the following are obtained using PBC, in order to treat a larger number of sites, however we have also checked

that open boundary conditions do not qualitatively alter the outcomes.

Let us now discuss the pairing term H_P in the total Hamiltonian (7):

$$H_P = \sum_{i,j=1}^{N_S} \Delta_{i,j} c_i^\dagger c_j^\dagger + \text{h.c.} \quad (14)$$

When both the pairing term $\Delta_{i,j}$ and the hopping term are nearest-neighbor ($\neq 0$ only if $j = i \pm 1$ and zero otherwise), then one has the Kitaev model [54]. Long-range in the pairings will be as well introduced:

$$\Delta_{i,j} \propto \frac{1}{|i-j|_p^\alpha}, \quad (15)$$

both with short-range and long-range hopping $t_{i,j}$. The full Hamiltonian, being quadratic, can be readily diagonalized [60], and we denote again by ϵ_k the corresponding eigenvalues. The EE of subsystems can be calculated from the matrices $t_{i,j}$ and $\Delta_{i,j}$, extending the result (12) valid when $\Delta_{i,j} = 0$. In the presence of pairings, indeed, the von Neumann entropy between two subsystems A and B , required to calculate the MI, has to be derived in a different way with respect to the case $\Delta_{i,j} = 0$ when one uses Eq. (12). With $\Delta_{i,j} \neq 0$ the correlations $\langle c_j c_l \rangle$ and $\langle c_j^\dagger c_l^\dagger \rangle$ do not vanish in general. We thus need to enlarge the correlation matrix to double its size in order to account for the additional terms. To do so, one define a matrix $M_{p,q} \equiv \langle (a_{2p-1}, a_{2p})(a_{2q-1}, a_{2q}) \rangle$, where $a_{2q-1} \equiv c_q + c_q^\dagger$ and $a_{2q} \equiv i(c_q - c_q^\dagger)$ are Majorana fermions, and the indices $p, q = 1, \dots, l$ run over the l sites of subsystem A . The matrix \mathbf{M} has l pairs of eigenvalues $1 \pm v_n$, in terms of which the EE is straightforwardly expressed as in (12). We refer to [55] for a presentation of the calculation of the EE for a generic quadratic form of fermions and for more references on the subject.

3. SHORT-RANGE MODELS

In this Section we consider short-range models, with nearest-neighbor hopping and $\Delta_{i,j} = 0$ (Sec. 3.1) or $\Delta_{i,j}$ nearest-neighbor as well (Sec. 3.2).

3.1. Tight-binding chain

The usual tight-binding chain Hamiltonian reads:

$$H = -t \sum_{i=1}^{N_S} c_i^\dagger c_{i+1} + \text{h.c.}, \quad (16)$$

with the PBC (8), so that $c_{N_S+1} = c_1$. We will consider an hopping term of the general form:

$$t_{i,j} = \frac{t}{|i-j|_p^\alpha}, \quad (17)$$

the nearest-neighbour case (16) being obtained for $\alpha \rightarrow \infty$.

The reason for considering (17) is two-fold: *i)* the short-range behaviour is in general expected to be retrieved for large, finite α ; *ii)* as discussed in [56], the EE of a subsystem does not depend on the exponent α . Indeed, the correlation matrix (13) can be written as $C_{i,j} = \sum_{l=1}^{N_T} \psi_l^*(i) \psi_l(j)$, where the ψ_α are the eigenfunctions of the matrix $t_{i,j}$. In the considered translational invariant case, the quantum number l becomes the wave vector k and the eigenfunctions ψ_l simply plane waves. So, if the dispersion relation ϵ_k has a purely monotonous behavior for k either positive or negative, then the correlation matrix is the same (since one has to sum on the *same* eigenfunctions). Thus, also the eigenvalues of the correlation matrix $C_{i,j}$ are equal and so are the EE and, therefore, the MI as well.

Since for any α in (17) the dispersion relation is indeed monotonous for k either positive or negative, as seen in the inset of Fig. 1, the MI does *not* depend on α . The main findings, valid therefore for any positive α in (17) and in particular for the short-range hopping model (16), are shown in Fig. 1 and Fig. 2. In Fig. 1 we plot the MI as a function of x . We see that the MI as a function of x has a linear behavior for small x and it is a monotonous function of x .

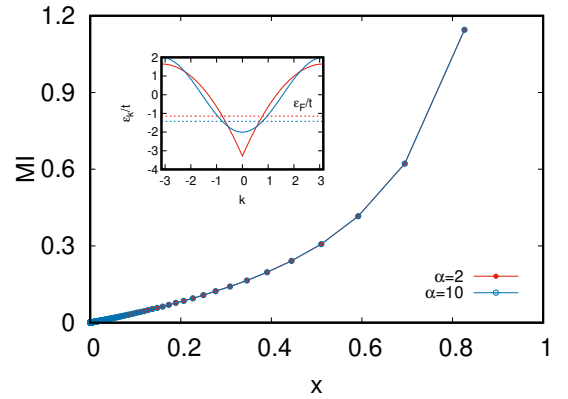


FIG. 1: Plot of the MI as a function of the conformal four-point ratio (6) for the hopping $t_{i,j} = t/|i-j|_p^\alpha$ in the Hamiltonian (9) and two different values of α : $\alpha = 2$ and $\alpha = 10$. As discussed in the text, checked numerically and seen in the figure, the MI does not depend on α , and it is the same for the short-range limit (16). The plot refers to a chain of length $N_S = 2004$, with PBC and filling fraction $f = 0.25$. The four-point ratio is calculated varying the distance between two subsystems of the same length $l = 10$. Inset: the two corresponding dispersion relations ϵ_k (in units of t) for $\alpha = 2$ and $\alpha = 10$, depicted together with their Fermi level. One sees that, even if the Fermi energies are different, the filled states are the same and, as a consequence, the MI is the same.

In Fig. 2 the MI is reported for different values of the

subsystems sizes l at fixed N_S and the same behavior appears for the considered cases. As supported also from simulations where the total length of the chain is varied, it is seen that the curves tends to converge to a monotonic function.

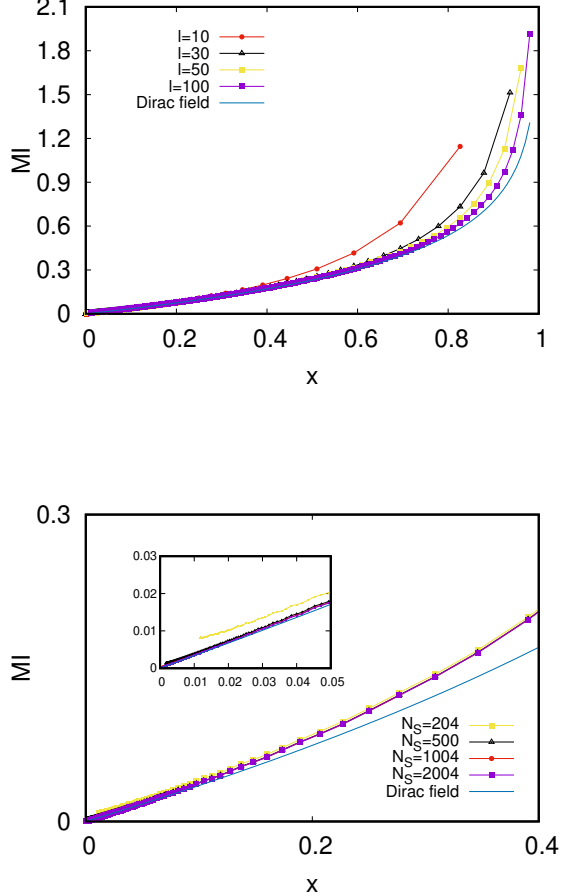


FIG. 2: Top panel: MI for the chain (9) with hopping (17) with $\alpha = 2$ and $N_S = 2004$ for several values of the subsystem size l . Bottom panel: Scaling of MI with the number of sites N_S for $l = 10$.

These results can be compared with the analytical values of the EE for disjoint subsystems of Dirac fermions, see [31] and refs. therein. This is done again in Fig. 2: the analytical values, given by

$$I = \frac{1}{3} \log \left(\frac{1}{1-x} \right), \quad (18)$$

are represented by the blue continuous line. We find a strongly improving agreement between numerics and analytics as l increases. Moreover, for fixed l , a very good stability of the data is achieved for $N_s \sim 1000$.

Further analytical results would be desirable to determine the MI as a function of x for intermediate and

large values of N_S, l, d at fixed filling to discuss finite-size corrections, however from the results presented here it emerges that x is the good quantity to use, the MI being a monotonic function of x . The prediction (5) is clearly not verified, as expected.

3.2. Kitaev chain

We consider in this Section the Kitaev Hamiltonian

$$H = -t \sum_{i=1}^{N_S} (c_i^\dagger c_{i+1} + \text{h.c.}) + \frac{\Delta}{2} \sum_{i,j=1}^{N_S} \frac{1}{|i-j|_p^\alpha} (c_j^\dagger c_i^\dagger + c_i c_j). \quad (19)$$

focusing on the limit $\alpha \rightarrow \infty$. In this limit, one recovers the short-range Kitaev chain [54], that in turn can be mapped via Jordan-Wigner transformations to the SR Ising model in transverse field [61].

For the model (19), it is convenient to work with anti-periodic boundary conditions [43]. To compare with previous results, without loss of generalities, we will set $\Delta = 2t = 1$ [43, 44], therefore measuring the energies in units of $2t$. To fix the number of particles, we introduce a chemical potential by adding the term $-\mu \sum_{j=1}^{N_S} (c_j^\dagger c_j - \frac{1}{2})$ to the Hamiltonian (19).

Presenting the results also for finite α , the spectrum of excitations is obtained via a Bogoliubov transformation and it results in:

$$\epsilon_k = \sqrt{(\mu - \cos k)^2 + f_\alpha^2(k + \pi)}, \quad (20)$$

where $k = -\pi + \frac{2\pi}{N_S} (n + \frac{1}{2})$ ($0 \leq n < N_S$) and

$$f_\alpha(k) \equiv \sum_{m=1}^{N_S-1} \frac{\sin(mk)}{|m|_p^\alpha}. \quad (21)$$

The functions $f_\alpha(k)$ become, in the thermodynamic limit [44, 47], a polylogarithmic function [62–64]. The ground state of Eq. (19) is given by

$$|\Omega\rangle = \prod_{n=0}^{N_S/2-1} \left(\cos \theta_{k_n} - i \sin \theta_{k_n} a_{k_n}^\dagger a_{-k_n}^\dagger \right) |0\rangle, \quad (22)$$

where $\tan(2\theta_{k_n}) = -\frac{f_\alpha(k_n + \pi)}{\mu - \cos k_n}$ and it is even under the Z_2 fermionic number parity of the Hamiltonian [65, 66].

The spectrum in (20) displays a critical line at $\mu = 1$ for every α and a critical semi-line $\mu = -1$ for $\alpha > 1$ (and therefore in the short-range Kitaev model $\alpha \rightarrow \infty$ as well).

We report in Fig. 3 the MI as a function of the conformal four-point ratio x for $\alpha = 1000$, practically indistinguishable from the short-range Kitaev model at $\alpha \rightarrow \infty$, $N_S = 1000$ and $\mu = 1.5$. In the inset of Fig. 3, we plot the corresponding spectrum ϵ_k for the Bogoliubov quasiparticles. In the considered ranges for the Hamiltonian parameters, the model satisfies an area law for

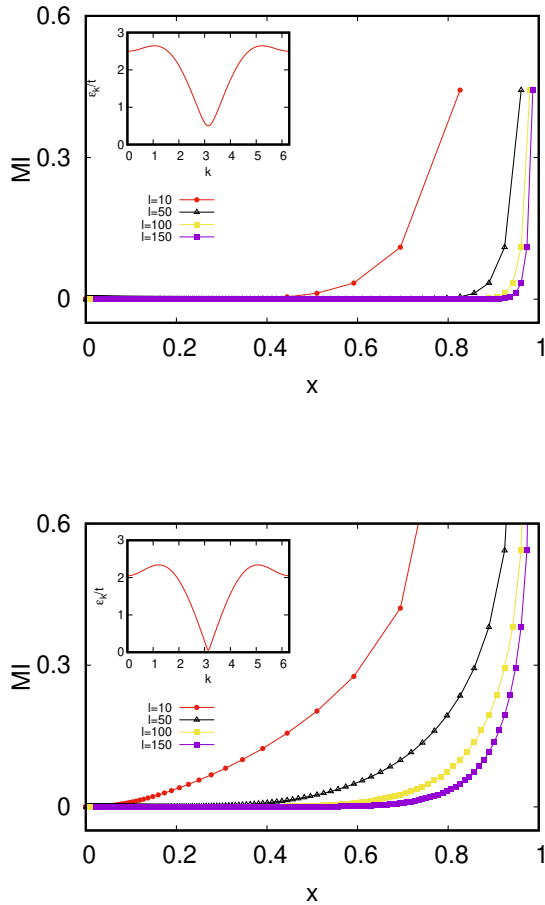


FIG. 3: (Upper panel) Bogoliubov quasiparticle spectrum (inset) and MI as a function of the four-point ratio x for the Kitaev chain (19) with $\alpha = 1000$, using the parameters $N_S = 2004$ and $\mu = 1.5$ (corresponding to the filling $f = 0.5567$). (Lower panel) Same, but for $\mu = 1.05$.

the EE, and correspondingly the MI appears to vanish for $x < 1/2$, in agreement by the AdS/CFT formula (5). However, the region in which MI vanished further $1/2$ approaching the thermodynamic limit

Finally, studying of the MI on the massless line $\mu = 1$, one finds a monotonic growth of the MI with x , qualitatively equal to those in Figs. 1 and 2, and corresponding to a logarithmic violation of the area law by the von Neumann entropy. For completeness, in Fig. 3 we also report the MI close to the critical line (choosing $\mu = 1.05$)

4. LONG-RANGE HOPPING

In this Section we consider models with long-range hopping.

For the model (9), without pairing terms ($\Delta_{i,j} = 0$)

and long-range hopping (17) given by $t_{i,j} = t/|i - j|^\alpha$, one can readily determine the energy spectrum as

$$\epsilon_k = -2t \ell_\alpha(k), \quad (23)$$

where $k = 2\pi n_k/N_S$ belongs to the first Brillouin zone ($n_k = -N_S/2, \dots, N_S/2 - 1$) and

$$\ell_\alpha(k) = \sum_{n=1}^{\infty} \frac{\cos(nk)}{n^\alpha}. \quad (24)$$

As commented in Sec. 3.1, the dispersion relation (23) is monotonous in k as in the short-range (see the inset of Fig. 1). The long-range hopping (17) only changes the values of the single-particle energies, and the MI is exactly the same of the short-range model, as discussed in Sec. 3.1 and illustrated in Figs. 1-2. We conclude that long-rangeness is not enough to change the MI properties, one also needs (if pairing terms are absent) to change the behavior of the single-particle spectrum, and, in particular, the Fermi surface. This is discussed in the next Section.

4.1. Fractal Fermi surface

We assume here that the Hamiltonian is such that the single-particle energy spectrum has the form

$$\epsilon_k = -t \sin\left(\frac{1}{k^\gamma}\right), \quad (25)$$

where γ is a positive odd integer. As shown in [56], at certain fillings, the Fermi surface of this model has a fractal topology. For instance, at half-filling $f = 0.5$, the Fermi energy is zero, with the point $k = 0$ being an accumulation point, see Fig. 4. The Fermi surface has box counting dimension $d_{box} = \frac{\gamma}{\gamma+1}$, so that $d_{box} = 1/2$ for $\gamma = 1$. From finite size numerical data one sees that the EE violates the area law as $S_A \sim L^\beta$, where $\beta = d_{box}$ [56].

Our results for the MI are reported in Figs. 4-6. The observed behavior differs from the previous models considered and displays very peculiar and unique features at small x . In Fig. 4 the MI as a function of x is shown at a fixed value of γ . It is seen that the non-logarithmic violation of the area law makes the MI non-monotonous at small x . In Fig. 5 we plot the results obtained for different sizes of the subsystem size l : the MI does not seem to be dependent solely on the conformal four-point ratio x , since, in this model, varying the subsystems length produces different outcomes. Moreover, a non-logarithmic violation of the area law violates the basic assumption of holography and thus we cannot expect Eq. (5) to apply here, since both conformal invariance and AdS/CFT duality are not respected. Our numerical results support this conclusion. In Fig. 6 the MI is plotted for different values of γ , *i.e.* of the exponent β quantifying the deviation from the area law. It is found that the larger is this

deviation, the more non-monotonic the MI is. This figure also indicates that the Bell-pairs responsible for the EE have a specific distribution in space also at very large distances.

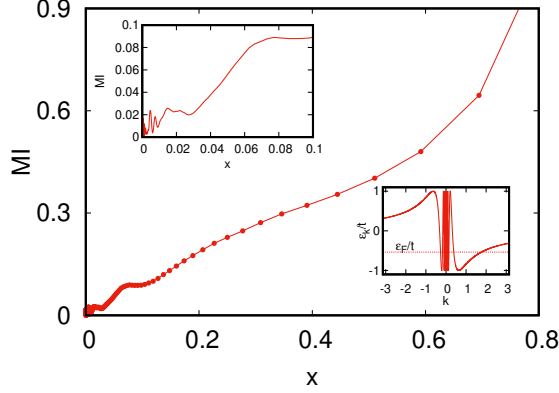


FIG. 4: Plot of the MI as a function of the conformal four-point ratio x for the chain with dispersion (25) and $\gamma = 1$, $f = 0.25$ and $N_S = 1004$. The four-point ratio is calculated varying the distance between two subsystems of the same length $l = 10$. In the top-left inset the small- x region is enlarged. In the bottom-right inset dispersion is plotted with the Fermi level (dotted line).

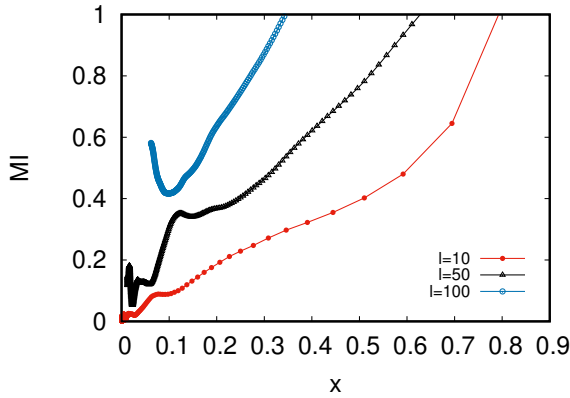


FIG. 5: MI vs x for the chain with dispersion (25) and $\gamma = 1$, $f = 0.25$ and $N_S = 1004$. The four-point ratio is calculated varying the distance between two subsystems of the same length $l = 10, 20, 50$.

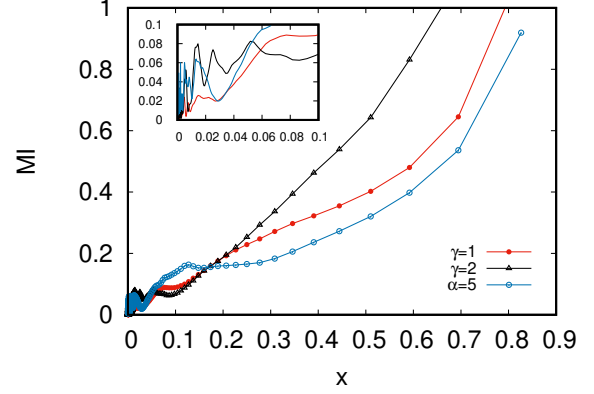


FIG. 6: MI vs x for the chain with dispersion (25) and $f = 0.25$, $N_S = 1004$ for different values of γ . The four-point ratio is calculated varying the distance between two subsystems of the same length $l = 10$. In the top-left inset the small- x region is enlarged.

4.2. Other models with non-logarithmic violations of the area law

Other models exhibiting non-logarithmic violations of the area law are considered in the following Sections 4.2.1 and 4.2.2. In both cases the pairing terms are absent, their effect being studied in Sec. 5.

4.2.1. Long-range power-law model with a phase

A possible way to modify the structure of the Fermi surface, is to introduce a space-dependent phase in the hopping matrix

$$t_{i,j} = \begin{cases} 0 & i = j, \\ \frac{te^{i\phi d(i-j)}}{|i-j|_p^\alpha} & i \neq j, \end{cases} \quad (26)$$

where $\phi = \frac{2\pi}{N_S}\Phi$ (with Φ a constant) and $d(m)$ is the oriented distance, defined as

$$d(m) \equiv \begin{cases} m & |m| \leq N_S - |m|, \\ -N_S + |m| & \text{otherwise.} \end{cases} \quad (27)$$

The energy spectrum is found to be $\epsilon_k = -2t\ell_\alpha(k)$ with

$$\ell_\alpha(k, \phi; N_S) = \sum_{n=1}^{N_S/2} \frac{\cos[n(k + \phi)]}{n^\alpha}. \quad (28)$$

While for $\phi = 0$ this function is monotonic for $k \in [0, \pi]$, for non-zero ϕ there is a critical value of $\alpha_c(\phi) < 1$ such that for $\alpha < \alpha_c(\phi)$, at half filling $f = 1/2$, the energies (28) are rapidly oscillating and the momenta k are

occupied in an alternating way between even and odd quantum numbers, as depicted in the right panel of Fig. 7. As a consequence, a Bell-paired-like ground state is obtained, with a volume law EE [56]. We notice that for $\alpha \leq 1$ the ground-state energy in the thermodynamic limit diverges. Nonetheless, one can make the energy extensive by the so-called Kac rescaling [57]. As reported in Fig. 7, the MI shows a non-monotonic behavior with x , emerging at small x (see left inset), where peaks develop. One also see a clear peak at $x \rightarrow 0$. We attribute the presence of such non-monotonicity and peaks to the formation of Bell pairs, which are the reason of the (non-logarithmic) deviation from the area law. This will be more evident in the models studied in the following Sec. 4.2.2. Also for the long-range power-law model with a phase, as for the model of Sec. 4.1, the four-point ratio x is found to be not sufficient to capture the whole structure of the MI, since as illustrated in Fig. 8, results with different values of l but the same x exhibit different results for the MI. However, non-monotonous behaviour and the increase for $x \rightarrow 0$ are seen.

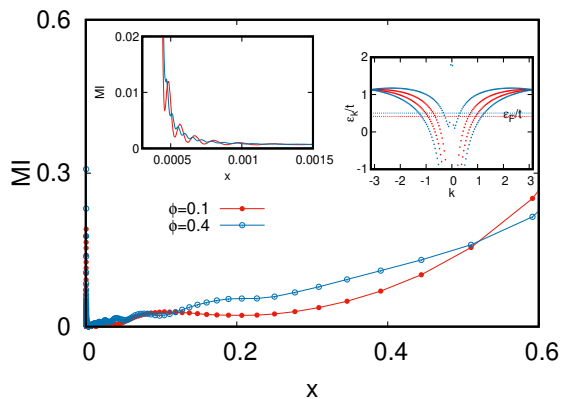


FIG. 7: MI for the long-range model (9) with the phase-modulated hopping (26) with two values of the phase $\phi = 0.1, 0.4$ and parameters $N_S = 1004$, $\alpha = 0.3$, $l = 10$, $f = 0.25$. Left inset: MI behaviour for small x . Right inset: energy spectrum for the two values of ϕ .

4.2.2. Selective hopping

We study in this Section the "antipodal" model in which each-site is connected via an hopping term to the more distant site in the chain (at the antipodes). This model has a maximally entangled ground-state with the maximum number of Bell pairs, and it exhibits perfect volume law [56]. To understand the role of deviations from (this time) volume law, we consider a chain with supplementary selective long-range hoppings, where the particle can only hop between sites centered around two

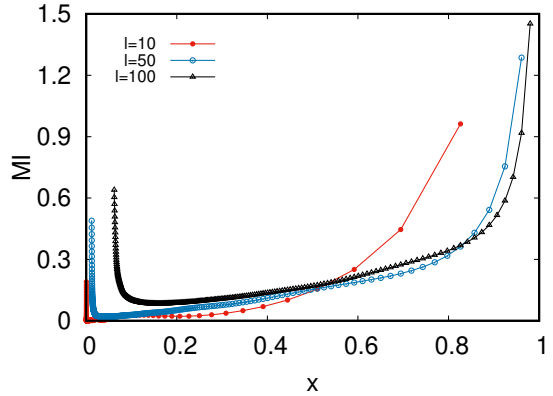


FIG. 8: MI for the long-range model (9) with the phase-modulated hopping (26) for $N_S = 1004$, $\alpha = 0.3$, $f = 0.25$, $\phi = 0.1$ and different values of l .

distances, denoted by $s_{1,2}$, in a window of $2r + 1$ sites (r being an integer). The Hamiltonian reads

$$H = - \sum_{j=1}^{N_S} \sum_{q=-r}^r \left(t_1 c_j^\dagger c_{j+s_1+q} + t_2 c_j^\dagger c_{j+s_2+q} + \text{h.c.} \right), \quad (29)$$

where PBC are implied. This model is readily diagonalized in Fourier space, with energies

$$\epsilon_k = -2 \left[t_1 \cos(ks_1) + t_2 \cos(ks_2) \right] \cos(kr) \left[1 + \frac{\tan(kr)}{\tan(k/2)} \right]. \quad (30)$$

We now look at the MI for three specific cases:

Antipodal Hopping: $s_1 = N_S/2$, $t_2 = 0$ ($t_1 = t$): Let set first $r = 0$ (pure antipodal hopping). This means that we allow particles to hop only between the antipodal points and back (again, we take N_S to be an even number). The single-particle spectrum reduces to

$$\epsilon_k = -2t \cos\left(\frac{kN_S}{2}\right) = -2t(-1)^{n_k}, \quad k = \frac{2\pi}{N_S} n_k, \quad (31)$$

which shows that there are two branches in the flat dispersion, with positive (negative) energy for odd (even) wave numbers. At half-filling, we thus have an alternating Fermi surface and a EE blue ruled by a (perfect) volume law. In fact, this choice of parameters creates a long-range Bell-paired state of maximal EE, since each particle is delocalized between two sites half-system apart. Remarkably, we find that such high entanglement content does not translate into the MI, which is in fact vanishing for any value of x . This can be explained as a reflection of the entanglement monogamy [67, 68] of the model. Thus, one needs systems with a lower EE.

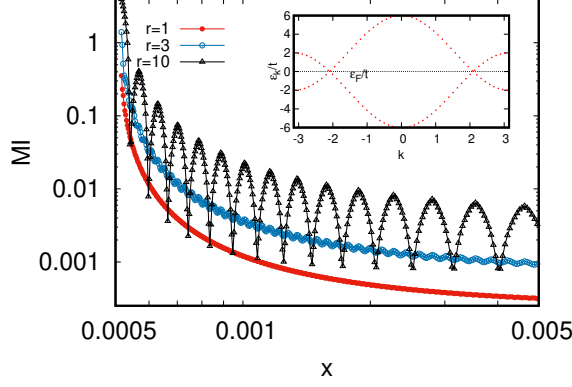


FIG. 9: MI for the antipodal hopping model (29), with $s_1 = N_S/2$ and $s_2 = 0$ and different values of $r = 1, 3, 10$. The case with $r = 1$ has a lower EE with respect to $r = 0$, but a larger MI and a corresponding peak for $x \simeq 0$. Increasing r increases the MI, and creates more peaks. Inset: energy spectrum for $r = 1$.

Allowing for $r \neq 0$ reduces the EE. For $r = 1$ one has

$$\epsilon_k = -2t(-1)^{n_k} \left[1 + 2 \cos \left(\frac{2\pi}{N_S} n_k \right) \right]. \quad (32)$$

Fig. 9 displays the MI for this case. We see that the reduction in EE corresponds to a peak of MI close to $x \simeq 0$, vanishing otherwise. Increasing r , the MI increases and more peaks are seen, as shown in Fig. 9 for $r = 3$ and 5.

Single hopping with $s_1 = s$, $t_2 = 0$ ($t_1 = t$): Here we have the dispersion relation

$$\epsilon_k = -2t \cos \frac{2\pi s n_k}{N_S} \quad (33)$$

with $r = 0$, and

$$\epsilon_k = -2t \cos \left(\frac{2\pi s n_k}{N_S} \right) \left[1 + \frac{\tan \left(\frac{2\pi r n_k}{N_S} \right)}{\tan \left(\frac{\pi n_k}{N_S} \right)} \right] \cos \left(\frac{2\pi r n_k}{N_S} \right) \quad (34)$$

for general r , from which the Fermi surfaces can be worked out. The EE violates the area law and the MI is plotted for different values of s_1 in Fig. 10 for $r = 0$. Similar results are found for other values of r (not reported). One sees that there is a single peak over a zero constant background corresponding to the Bell pair at the given s_1 . The position of this peak moves toward $x \simeq 0$ in the thermodynamic limit, similarly to what observed in Fig. 9.

Hopping exactly to two distant sites with $r = 0$: With hopping allowed only between sites with distances s_1 and s_2 , one has

$$\epsilon_k = -2 \left[t_1 \cos \left(\frac{2\pi s_1 n_k}{N_S} \right) + t_2 \cos \left(\frac{2\pi s_2 n_k}{N_S} \right) \right]. \quad (35)$$

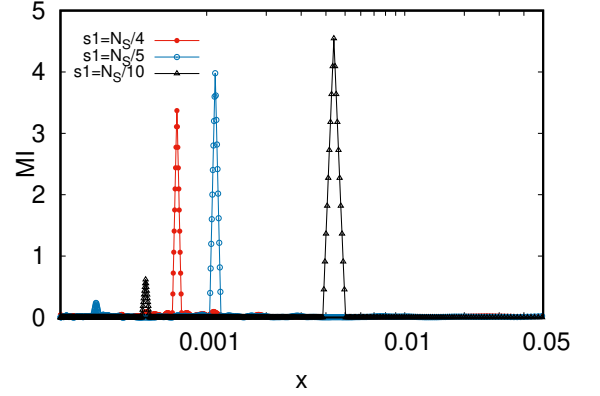
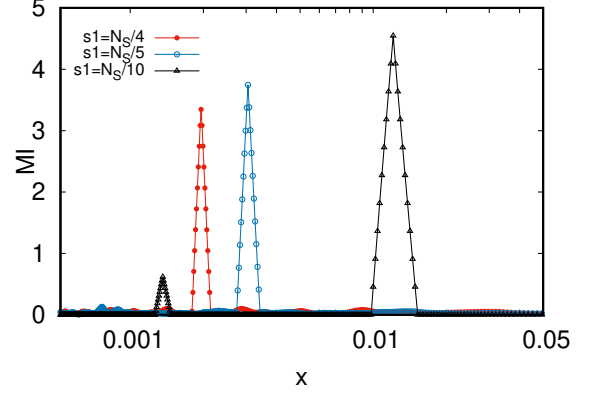


FIG. 10: MI for the selected hopping model (29) with $t_2 = 0$, $f = 0.5$, $r = 0$ and different values $s_1 = N_S/4, N_S/5, N_S/10$. We consider different chain lengths $N_S = 900$ (top panel) and 1500 (bottom panel). The only peaks on a zero background move toward $x \simeq 0$ in the thermodynamic limit

For $s_1 = N_S/2$ and $s_2 = N_S/4$ at half-filling $f = 1/2$, the single-particle spectrum is following a zig-zag behaviour, with odd wavenumber states filled in the ground state. As for the case of Fig. 9, this is a maximal EE case, where two-particles are delocalized over 4 sites ($N_S/4$ apart), and the MI vanishes. In Fig. 11 we show the MI for and $s_1 = N_S/4, s_2 = N_S/5$ at half-filling $f = 1/2$. The EE is lowered, but the MI shows peaks for small x , related to the corresponding Bell pairs.

We also considered the case $s_1 = N_S/2 - 1, s_2 = N_S/2 + 1$ ($t_1 = t_2 = t$) with $r = 0$, i.e.

$$H = -t \sum_j \left(c_j^\dagger c_{j+\frac{N}{2}+1} + c_j^\dagger c_{j+\frac{N}{2}-1} + \text{h.c.} \right), \quad (36)$$

with single-particle spectrum

$$\epsilon_k = -4t(-1)^{n_k} \cos \frac{2\pi}{N} n_k. \quad (37)$$

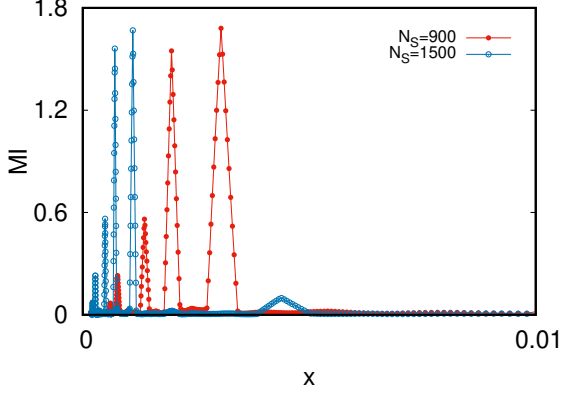


FIG. 11: MI for the selected hopping model (29) from any site only to two distant sites ($r = 0$ and $f = 0.5$) $s_1 = N_S/4$ and $s_2 = N_S/5$.

The MI is depicted in Fig. 12 and shows similarities with the case in Fig. 7, where one has indeed a volume law, but not the perfect (i.e., maximal) volume law.

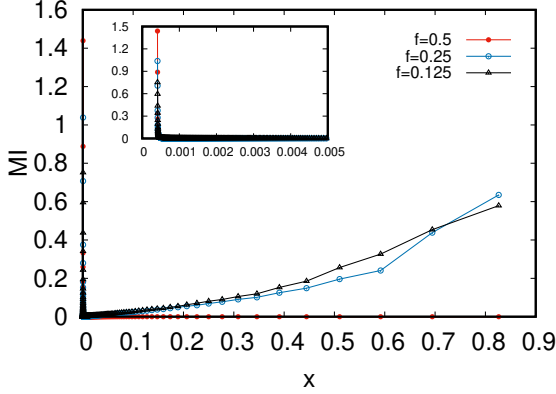


FIG. 12: MI for the model (29) with hopping from any site only to the two sites surrounding the antipodal point ($s_{1,2} = N_S/2 \pm 1$), with the right panel zooming the small x behavior.

5. LONG-RANGE KITAEV CHAINS

We consider in this Section the effect of a long-range counterpart of the fermionic pairing as given in Eq.(14), both in the presence of short-range (Sec. 5.1) and long-range (Sec. 5.2) hopping.

5.1. Short-range hopping and long-range pairing

Let us consider here long-range pairing ($\Delta_{i,j} = \Delta/2|i-j|^\alpha$) and nearest-neighbour hopping ($t_{i,j} = t$ only if $i = j \pm 1$ and zero otherwise). The MI for the limit $\alpha \rightarrow \infty$ have been discussed in Sec. 3.2, where we also reported the energy spectrum for finite α in Eq. (20). As in Sec. 3.2 we consider $\Delta = 2t$.

We remind that the spectrum (20) displays a critical line at $\mu = 1$ for every α and a critical semi-line $\mu = -1$ for $\alpha > 1$. Moreover, if $\mu \neq -1$ the velocity of quasi-particle with $k = \pm\pi$ diverges if $\alpha \leq \frac{3}{2}$, while it diverges at $\alpha \leq 2$ if $\mu = -1$ [43]. Below $\alpha = 1$ and at every value of μ , new phases occur [43, 69, 70]. There, the area law for the EE is logarithmically violated [69, 71]. Moreover the boundary Majorana modes, present above $\alpha = 1$ if $|\mu| < 1$, become massive and disappear. Notably, this transition to the new phases at $\alpha = 1$ occurs without any mass gap closure, as a consequence of the large space correlations induced by the LR pairing. This transition is signaled by the ground-state fidelity [70].

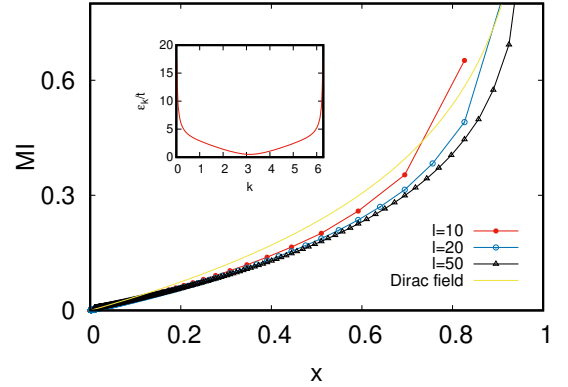


FIG. 13: MI as a function of the four-point ratio x for the long-range Kitaev model with $\alpha = 0.5$ and short-range hopping, with $N_S = 1000$, $\mu = 1.5$ (corresponding to an average occupation filling $f = 0.5567$). Inset: Bogoliubov quasiparticle spectrum.

Also for the MI, qualitatively different results are found passing through the line $\alpha = 1$. We report in Fig. 13 the MI, as a function of the conformal four-point ratio x for $\alpha = 0.5$, for a closed chain with length $N_S = 1000$ and $\mu = 1.5$. In the inset, we plot the Bogoliubov spectrum ϵ_k . For $\alpha \gtrsim 1$, the model satisfies an area law for the EE and the MI is qualitatively similar to that of Fig. 3: it appears to be vanishing for small x . Instead, for $\alpha \lesssim 1$, the EE is logarithmically violated, and the MI increases monotonically with x , qualitatively similar to that in Eq. (13). This is not due to the fact the model is gapless (see the inset), but rather to the fact that it has a so long-ranged pairing that the correlation functions

are power-law decaying. This make the MI of the system similar to the tight-binding model studied in Sections 3.1 and 4.

Around the line $a = 1$, the change of behaviour is smooth at finite size N_s , similarly as the EE [43]. This behaviour is shown in Fig. 14. There MI at for a value of x near 1/2 is reported. Finally, on the massless line

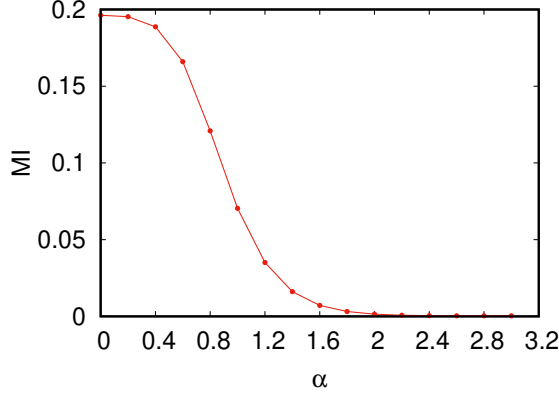


FIG. 14: MI at $x = 0.484$ for the long-range Kitaev model with $\alpha = 0.5$ and short-range hopping, with $N_s = 200$, and $\mu = 1.5$.

$\mu = 1$, also at $\alpha < 1$, we find again a monotonic growth of the MI with x , similar to the short-range Kitaev chain.

In Fig. 13 a comparison is made again the analytical values of the EE for disjoint subsystems of Dirac fermions. We find that the agreement is rather poor. However, this mismatch is of course expected, since a Dirac structure does not hold for $\alpha < 2$, not even around the massless (semi-) lines at $\mu = \pm 1$, where conformal invariance is broken by the long-range coupling [47]. We recall that instead the same Dirac structure holds around $\mu = \pm 1$ and for $\alpha > 2$ [65].

The MI can be used to detect quantum phase transitions. To show this, we keep the four-point ratio fixed and swipe for the phase-diagram parameters μ and α . In Fig. 15 we show in the upper panel the MI as a function of μ for a chain with length $N_s = 1000$, $l = 16$, $d = 4$, and $\alpha = 10$. Two peaks are observed at $\mu = \pm 1$, in correspondence to the two critical points. Similarly, in the left panel we report the MI *vs* μ for $\alpha = 0.5$ and the same choices for the other parameters. We observe a single peak, in correspondence to the unique critical point at $\mu = 1$.

In Fig. 16 we plot the MI *vs* α for $\mu = 0.5$ and $\mu = 2.5$, and the other parameters as before. We observe a substantial increase for the MI for $\alpha \lesssim 1$, in correspondence to the two LR phases in this regime, where the area law for the von Neumann entropy is logarithmically violated [43, 69]. Finally, for completeness we report in Fig. 17

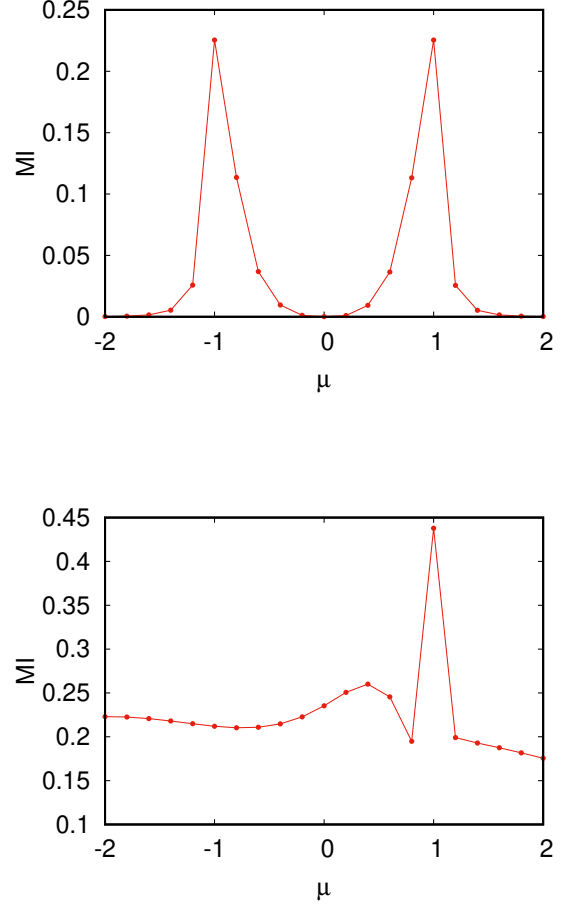


FIG. 15: MI as a function of the chemical potential μ for the Kitaev chain with long-range pairing and short-range hopping with $\alpha = 10$ (top) and $\alpha = 0.5$ (bottom) and $N_s = 1000$, $l = 16$, $d = 4$ sites.

the filling *vs* the chemical potential for different values of α .

5.2. Long-range hopping and pairing

We finally consider the long-range paired Kitaev model with also long-range hopping:

$$H = - \sum_{i,j=1}^{N_s} \frac{t}{|i-j|_p^\beta} \left(c_i^\dagger c_j + \text{h.c.} \right) - \sum_{i,j=1}^{N_s} \frac{\Delta}{2|i-j|_p^\alpha} \left(c_j^\dagger c_i^\dagger + c_i c_j \right), \quad (38)$$

where we denote by β (α) the power-law decay exponent of the hopping (pairing) term.

We plot in the in Figs. 18 and 19 the MI as a function of x for two different values of the pair α, β (with $N_s = 1000$ and $\mu = 1.5$). In the insets of both the panels, the corresponding energy spectrum is plotted. In Fig.

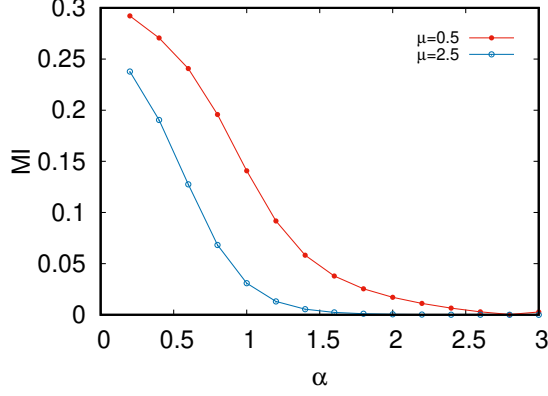


FIG. 16: MI as a function of the power of long-range decay α of the pairing for $\mu = 0.5$ (left) and $\mu = 2.5$ (right) with $N_S = 1000$, $l = 16$, $d = 4$ sites.

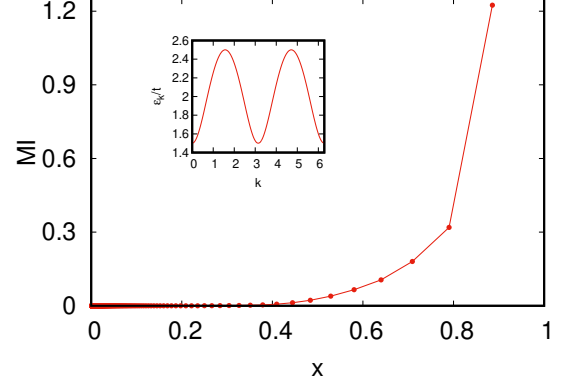


FIG. 18: MI *vs* x for the Kitaev chain (38) with non-local hopping and pairing. The parameters $\alpha = 100$ and $\beta = 0.5$, with $N_S = 1000$ and $\mu = 1.5$, are used. Inset: Bogoliubov quasiparticle spectrum.

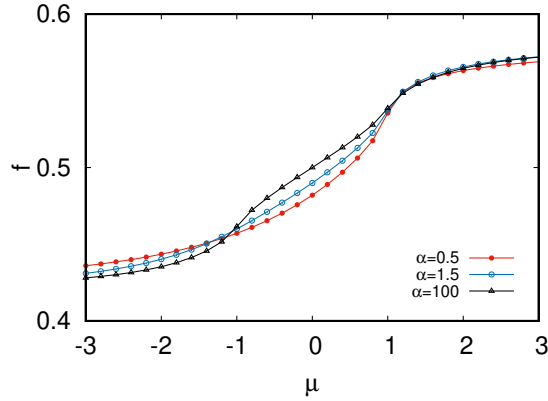


FIG. 17: Filling versus chemical potential for different values of α .

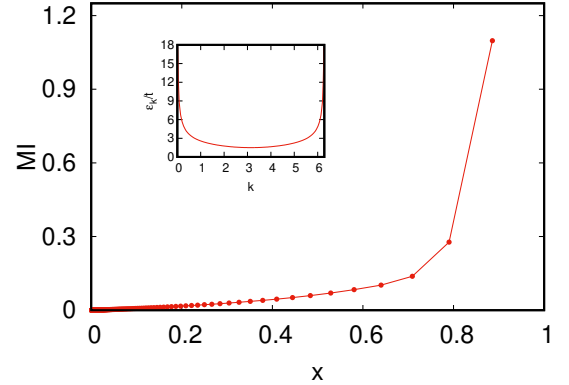


FIG. 19: Same as in Fig. 18, but here $\alpha = \beta = 0.5$.

18 we consider $\alpha = 100$ and $\beta = 0.5$, corresponding to a choice of short-range pairing and long-range hopping. In this case, it is seen that the spectrum of the Bogoliubov quasiparticles is regular, not fractal or "zig-zag", like the ones studied in Sections 4.1 and 4.2. The MI is vanishing for small x , paralleling the fulfill of area law for the EE, and conforming the obtained results for the short-range Kitaev model. Instead, the case $\alpha = \beta = 0.5$, with both hopping and pairing long-range, is considered in Fig. 19. In this case, there are logarithmic violations for the EE area law and, correspondingly, we find that the MI is a monotonously increasing function of the conformal four-point ratio x , similar to the behaviors on massless semi(lines) $\mu \pm 1$, or in the regime $\alpha < 1$, of the model in Eq. (19).

6. CONCLUSIONS

We have studied the mutual information (MI) for several quadratic fermionic chains with a variety of different long-range hoppings and superconductive pairings, including the Kitaev model with short- and long-range pairings and the antipodal model in which the hoppings connect the most distant sites of the chain. The MI has been plotted as a function of the conformal four-point ratio x .

The conclusions emerging from the considered examples are the following. 1) When the area law is obeyed at most with logarithmic corrections, the MI is a monotonically increasing function of x , going to zero for $x \rightarrow 0$. 2) In these cases, x appears as a convenient variable, in the

sense that different values of the sizes of the system, of the subsystems and their distance with the same x produces for large sizes the same value of x . 3) When there are non-logarithmic violation of the area law, the behaviour of MI *vs* x is no longer monotonic and peaks appear, with the exception of the antipodal model in which MI vanishes identically, corresponding to a perfect, maximal volume law for the bipartite EE. 4) In these cases x does not capture the structure of the MI, since parameters with the same x do not have the same x (even though a similar qualitative behaviour is found).

The short-range Kitaev model in the massive regime exhibits a behaviour such that the MI is vanishing for small values of x , similarly to what happens to the AdS/CFT prediction (5). This result is actually independent from the short or long-range nature of the hopping. When the pairing becomes strongly long-range ($\alpha < 1$), then the MI is no longer vanishing for small x due to the power-law nature of the correlations induced by the long-range pairings. We point out that, as expected, for the Kitaev model we did not find a good agreement between our results for larger values of x (say $x \gtrsim 1/2$) and the AdS/CFT prediction (5), since the latter is valid in the strong coupling limit. However, in both cases there is an overall monotonic growth of the MI as a function of the conformal four-point ratio x . For the considered Kitaev models, we showed the possibility to locate phase transitions using MI. Keeping the four-point ratio constant and sweeping the phase diagram, the MI displays distinct peaks at the closings of the gap, as shown in Figs. 15 and 16.

We also analyzed the MI behavior in systems with volume-like violations of the area law. We observed the emergence of peaks, and in particular for $x \simeq 0$, reflecting the structure of shared Bell-pairs between the subsystems. In fact, violations of the area law imply the formation of Bell pairs at arbitrary distances, growing with the thermodynamic limit. From this point of view we can then expect that in the infinite chain length limit, these peaks get squeezed toward $x \rightarrow 0$ (see Fig. 10). To analyze this behaviour we considered models with a controllable deviation from the perfect (i.e., maximal) volume law exhibited by the antipodal model. For the case of maximal volume law EE we found a vanishing MI

(which can also be interpreted as a sign of entanglement monogamy) when the EE decreases the MI increases and peaks appear. The distribution of the latter is related to the formation of Bell-paired states at different distances, as it happens in the model with selective hopping considered in Sec. 4.2.2. A non-monotonic behaviour of the MI is observed, with features not being universal in terms of the four-point ratio. We can qualitatively explain this by the fact that a specific spatial distribution of Bell pairs cannot be simply captured by conformal invariant quantities.

The presented results show that the MI, even though not a proper entanglement measure, can be used to extract important information about the entanglement properties and the phases of a quantum system. The peculiar role of long-range terms, as intertwined with the possible occurrence of violations of the area law, have been investigated and shown to produce a variety of interesting features. It would be certainly very interesting both to find analytical results for the behaviour of MI as a function of the conformal four-point ratio for some of the models considered here and to extend the analysis of the MI to interacting, non-quadratic models. Indeed, our results show that already for systems that can be mapped to free fermions the MI is not always captured by the existing analytical expressions.

ACKNOWLEDGEMENTS

The authors are pleased to thank Domenico Giuliano, Erik Tonni and Vladimir Korepin for useful discussions. L. L. acknowledges financial support by the PRIN project number 20177SL7HC, financed by the Italian Ministry of education and research. F. F. acknowledges support from the Croatian Science Foundation (HrZZ) Projects No. IP-2016-6-3347 and IP-2019-4-3321, as well as from the QuantiXLie Center of Excellence, a project co-financed by the Croatian Government and European Union through the European Regional Development Fund – the Competitiveness and Cohesion (Grant KK.01.1.1.01.0004).

-
- [1] P. Calabrese, J. Cardy, & B. Doyon (eds.), "Entanglement entropy in extended quantum systems - Special Issue", J. Phys. A **42** (2009).
 - [2] S. Rachel, M. Haque, A. Bernevig, A. Laeuchli, & E. Fradkin (eds.), "Quantum Entanglement in Condensed Matter Physics - Special Issue", J. Stat. Mech. (2015)
 - [3] J. Eisert, M. Cramer, and M. B. Plenio, Rev. Mod. Phys. **82**, 277 (2010).
 - [4] M. Wolf, F. Verstraete, M. Hastings, & J. Cirac, Phys. Rev. Lett. **100**, 070502 (2008).
 - [5] D. J. C. MacKay, Information Theory, Inference, and

- Learning Algorithms (Cambridge, Cambridge University Press, 2003).
- [6] J. Um, H. Park, & H. Hinrichsen, J. Stat. Mech. P10026 (2012).
- [7] H. W. Lau & P. Grassberger, Phys. Rev. E **87**, 022128 (2013).
- [8] F. C. Alcaraz & M. A. Rajabpour, Phys. Rev. Lett. **111**, 017201 (2013).
- [9] F. C. Alcaraz & M. A. Rajabpour, Phys. Rev. B **90**, 075132 (2014).
- [10] J.-M. Stéphan, Phys. Rev. B **90**, 045424 (2014).

- [11] R. G. Melko, A. B. Kallin, & M. B. Hastings, *Phys. Rev. B* **82**, 100409(R) (2010).
- [12] R. R. P. Singh, M. B. Hastings, A. B. Kallin, & R. G. Melko, *Phys. Rev. Lett.* **106**, 135701 (2011).
- [13] J. Wilms, M. Troyer, & F. Verstraete, *J. Stat. Mech.* (2011) P10011
- [14] J. Iaconis, S. Inglis, A. B. Kallin, & R. G. Melko, *Phys. Rev. B* **87**, 195134 (2013).
- [15] H. Bernigau, M. J. Kastoryano, & J. Eisert, *J. Stat. Mech.* P02008 (2015).
- [16] J. Schachenmayer, B. P. Lanyon, C. F. Roos, & A. J. Daley, *Phys. Rev. X* **3**, 031015 (2013).
- [17] V. Eisler & Z. Zimboras, *Phys. Rev. A* **89**, 032321 (2014).
- [18] C. T. Asplund & A. Bernamonti, *Phys. Rev. D* **89**, 066015 (2014).
- [19] V. Alba & P. Calabrese, *PNAS* **114**, 7947 (2017).
- [20] M. Gruber & V. Eisler, [arXiv:2001.06274](https://arxiv.org/abs/2001.06274)
- [21] S. Maity, S. Bandyopadhyay, S. Bhattacharjee, & A. Dutta, [arXiv:2001.09802](https://arxiv.org/abs/2001.09802)
- [22] J. C. Getelina, F. C. Alcaraz, & J. A. Hoyos, *Phys. Rev. B* **93**, 045136 (2016).
- [23] P. Ruggiero, V. Alba, & P. Calabrese, *Phys. Rev. B* **94**, 035152 (2016).
- [24] G. De Tomasi, S. Bera, J. H. Bardarson, & F. Pollmann, *Phys. Rev. Lett.* **118**, 016804 (2017).
- [25] A. Hamma, S. M. Giampaolo, & F. Illuminati, *Phys. Rev. A* **93**, 012303 (2016).
- [26] M. Headrick, *Phys. Rev. D* **82** 12 126010 (2010).
- [27] J. Molina-Vilaplana & P. Sodano, *J. High Energy Phys.* **2011**, 11 (2011).
- [28] A. Allais & E. Tonni, *J. High Energ. Phys.* **2012**, 102 (2012).
- [29] W. Fischler, A. Kundu, & S. Kundu, *Phys. Rev. D* **87**, 126012 (2013).
- [30] L. Brightmore, G. P. Geher, A. R. Its, V. E. Korepin, F. Mezzadri, M. Y. Mo, & J. A. Virtanen, [arXiv:1912.08658](https://arxiv.org/abs/1912.08658).
- [31] H. Casini and M. Huerta, *J. Phys. A* **42**, 504007 (2009).
- [32] P. Di Francesco, P. Mathieu, & D. Sénéchal, *Conformal field theory* (New York, Springer, 1997).
- [33] G. L. Celardo, R. Kaiser, & F. Borgonovi, *Phys. Rev. B* **94**, 144206 (2015).
- [34] Z. X. Gong, M. F. Maghrebi, A. Hu, M. Foss-Feig, P. Richerme, C. Monroe, & A. V. Gorshkov, *Phys. Rev. B* **93**, 205115 (2016).
- [35] N. Defenu, A. Trombettoni, & S. Ruffo, *Phys. Rev. B* **94**, 224411 (2016).
- [36] N. Defenu, A. Trombettoni, & S. Ruffo, *Phys. Rev. B* **96**, 104432 (2017).
- [37] F. Iglói F, B. Blaž, G. Roósz G, & H. Rieger, *Phys. Rev. B* **98**, 184415 (2018).
- [38] B. Blaž, H. Rieger, G. Roósz, & F. Iglói, *Phys. Rev. Lett.* **121**, 095301 (2018).
- [39] N. Defenu, T. Enss, M. Kastner, & G. Morigi, *Phys. Rev. Lett.* **121**, 240403 (2018).
- [40] L. Leroose, B. Zunkovic, A. Silva, & A. Gambassi, *Phys. Rev. B* **99**, 121112 (2019).
- [41] S. Pappalardi, P. Calabrese, & G. Parisi, *J. Stat. Mech.* 073102 (2019).
- [42] A. Leroose & S. Pappalardi, *Phys. Rev. Res.* **2**, 012041(R) (2020).
- [43] D. Vodola, L. Lepori, E. Ercolessi, A. V. Gorshkov, & G. Pupillo, *Phys. Rev. Lett.* **113**, 156402 (2014).
- [44] D. Vodola, L. Lepori, E. Ercolessi, & G. Pupillo, *New J. Phys.* **18**, 015001 (2016).
- [45] A. S. Buyskikh, M. Fagotti, J. Schachenmayer, F. Essler, & A. J. Daley, *Phys. Rev. A* **93**, 053620 (2016).
- [46] M. Van Regemortel, D. Sels, & M. Wouters, *Phys. Rev. A* **93**, 032311 (2016).
- [47] L. Lepori, D. Vodola, G. Pupillo, G. Gori, & A. Trombettoni, *Ann. Physics* **374**, 35 (2016).
- [48] A. Dutta & A. Dutta, *Phys. Rev. B* **96**, 125113 (2017).
- [49] L. Lepori, A. Trombettoni, & D. Vodola, *J. Stat. Mech.* 033102 (2017).
- [50] A. Alecce & L. Dell'Anna, *Phys. Rev. B* **95**, 195160 (2017).
- [51] N. Defenu, T. Enss, & J. C. Halimeh, *Phys. Rev. B* **100**, 014434 (2019).
- [52] N. Defenu, G. Morigi, L. Dell'Anna, & T. Enss, *Phys. Rev. B* **100**, 184306 (2019).
- [53] P. Urich, N. Defenu, R. Jafari, & J. C. Halimeh, *Phys. Rev. B* **101**, 245148 (2020).
- [54] A. Y. Kitaev, *Phys.-Uspekhi* **44**, 131 (2001).
- [55] I. Peschel, *Braz. J. Phys.* **42**, 267 (2012).
- [56] G. Gori, S. Paganelli, A. Sharma, P. Sodano, & A. Trombettoni, *Phys. Rev. B* **91** 245138 (2015).
- [57] A. Campa, T. Dauxois, D. Fanelli, & S. Ruffo, *Physics of long-range interacting systems* (Oxford, Oxford University Press, 2014).
- [58] J. Sak, *Phys. Rev. B* **8**, 281 (1973).
- [59] N. Defenu, A. Codello, S. Ruffo, & A. Trombettoni, *J. Phys. A* **53**, 143001 (2020).
- [60] J.-P. Blaizot & G. Ripka, *Quantum theory of finite systems* (Cambridge, MIT Press, 1986).
- [61] A. Dutta, G. Aeppli, B. K. Chakrabarti, U. Divakaran, T. F. Rosenbaum, & D. Sen, *Quantum Phase Transitions in Transverse Field Models* (Cambridge, Cambridge University Press, 2015).
- [62] I. S. Gradshteyn & I. M. Ryzhik, *Tables of Integrals, Series, and Products* (Amsterdam, Elsevier, 2007).
- [63] M. Abramowitz & I. A. Stegun, *Handbook of Mathematical Functions* (New York, Dover, 1964).
- [64] F. W. J. Olver, D. W. Lozier, R. F. Boisvert, & C. W. Clark, *NIST Handbook of Mathematical Functions* (Cambridge, Cambridge University Press, 2010).
- [65] G. Mussardo, *Statistical Field Theory: An Introduction to Exactly Solved Models in Statistical Physics* (Oxford, Oxford University Press, 2010).
- [66] P. Fendley, *J. Stat. Mech.* P11020 (2012).
- [67] V. Coffman, J. Kundu, & W. K. Wootters, *Phys. Rev. A* **61**, 052306 (2000).
- [68] T. J. Osborne & F. Verstraete, *Phys. Rev. Lett.* **96**, 220503 (2006).
- [69] L. Lepori & L. Dell'Anna, *New J. Phys.* **19**, 103030 (2017).
- [70] L. Pezzé, M. Gabbriellini, L. Lepori, & A. Smerzi, *Phys. Rev. Lett.* **119**, 250401 (2017).
- [71] F. Ares, J. G. Esteve, F. Falceto, & A. R. de Queiroz, *Phys. Rev. A* **92**, 042334 (2015).